



Piperazine clubbed with 2-azetidinone derivatives suppresses proliferation, migration and induces apoptosis in human cervical cancer HeLa cells through oxidative stress mediated intrinsic mitochondrial pathway

Rashmin Khanam¹ · Raj Kumar² · Iram Iqbal Hejazi¹ · Syed Shahabuddin³ · Ramovatar Meena² · Vikrant Jayant² · Prabhat Kumar² · Abdul Roouf Bhat⁴  · Fareeda Athar¹

© Springer Science+Business Media, LLC, part of Springer Nature 2018

Abstract

Piperazine scaffolds or 2-azetidinone pharmacophores have been reported to show anti-cancer activities and apoptosis induction in different types of cancer cells. However, the mechanistic studies involve in induction of apoptosis addressing these two moieties for human cervical cancer cells remain uncertain. The present study emphasizes on the anti-proliferating properties and mechanism involved in induction of apoptosis for these structurally related azoles derivatives in HeLa cancer cells. 1-Phenylpiperazine clubbed with 2-azetidinone derivatives (**5a–5h**) were synthesized, characterized using various spectroscopic techniques and evaluated for their in-vitro anti-proliferative activities and induction of apoptosis. Further, we also evaluated oxidative stress generated by these synthetic derivatives (**5a–5h**). Cell viability studies revealed that among all, the compound *N*-(3-chloro-2-(3-nitrophenyl)-4-oxoazetidin-1-yl)-2-(4-phenylpiperazin-1-yl) acetamide **5e** remarkably inhibited the growth of HeLa cells in a concentration dependent manner having IC₅₀ value of 29.44 ± 1.46 µg/ml. Morphological changes, colonies suppression and inhibition of migration clearly showed the antineoplasticity in HeLa cells treated with **5e**. Simultaneously, phosphatidylserine externalization, DNA fragmentation and cell-cycle arrest showed ongoing apoptosis in the HeLa cancer cells induced by compound **5e** in concentration dependent manner. Additionally, generation of intracellular ROS along with the decrease in mitochondrial membrane potential supported that compound **5e** caused oxidative stress resulting in apoptosis through mitochondria mediated pathway. Elevation in the level of cytochrome *c* and upregulation in expression of caspase-3 clearly indicated the involvement of the intrinsic pathway of programmed cell death. In brief; compound **5e** could serve as a promising lead for the development of an effective antitumor agent.

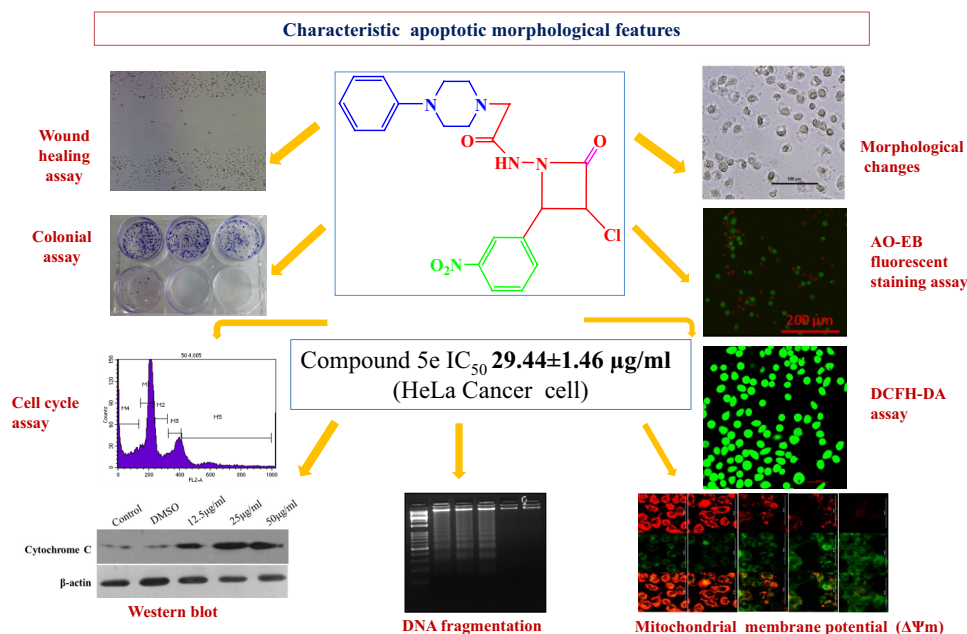
Electronic supplementary material The online version of this article (<https://doi.org/10.1007/s10495-018-1439-x>) contains supplementary material, which is available to authorized users.

✉ Abdul Roouf Bhat
abroouf@yahoo.co.in

✉ Fareeda Athar
fathar@jmi.ac.in

- ¹ Centre for Interdisciplinary Research in Basic Sciences, Jamia Millia Islamia, New Delhi 110025, India
- ² Radiation and Cancer Therapeutic Lab, School of Life Sciences, Jawaharlal Nehru University, New Delhi 110067, India
- ³ Research Centre for Nano-Materials and Energy Technology (RCNMET), School of Science and Technology, Sunway University, 47500 Selangor, Malaysia
- ⁴ Department of Chemistry, Sri Pratap College, Cluster University, Srinagar 190001, India

Graphical Abstract



Keywords Piperazines · 2-Azetidinones · Apoptosis · Anticancer activity · Oxidative stress

Abbreviations

MTT	3-(4,5-Dimethylthiazol-2-yl)-2,5-diphenyl-tetrazolium bromide
DCFH-DA	2',7'-Dichlorofluorescein diacetate
AO	Acridine orange
ROS	Reactive oxygen species
MMP	Mitochondrial membrane potential
RPMI	Roswell Park Memorial Institute medium

Introduction

Cervical cancer is the second most commonly occurring cancer and also a third leading cause of deaths among women worldwide [1]. There are several environmental elements like carcinogens, viruses, chemicals, radiations including germline mutations as one of the genetic factors that initiate cancer and progressively leads to malignant cells, invasion and metastasis. In spite of much substantial progress been made in the treatment of cervical cancer involving combinational therapies of surgery, chemotherapy and radiotherapy, the possibilities of remission, relapse and metastasis still exist in comparison to other types of cancer with mortality rate of 30% within 5 years of treatment [2].

Improper regulation of programmed cell death prominently contributes to both cancer development and drug responsiveness [3]. There are different gene families

regulating the apoptotic pathways leading to phagocytosis by neighboring cells. There are mainly two pathways, extrinsic death receptor pathway and mitochondrial (intrinsic) pathway involved in the execution of apoptosis [4]. Although inducing apoptosis through chemotherapy is one of the main approaches used in cancer treatment, but unfortunately many drugs used in chemotherapy suffer from various side effects and attain resistance [5]. Thus, in order to improve the clinical outcomes in cancer, new chemotherapeutics directing towards apoptosis transduction signals must be discovered [6].

Piperazine scaffolds areazole derivatives constituting important structural framework for many drugs backbones and displaying wide spectrum of biological activities like anti-oxidation and anti-inflammation [7]. Piperazines are of great significances since they act as specific ligands for many biological targets and also possess an elastic binding feature with common substrates [8]. Interacting with DNA is another distinct characteristic shown by the piperazine derivatives [9]. In addition to these, piperazines have been shown to exhibit anticancer [10], antifungal [11], antibacterial and antimalarial activities [12]. Piperazine derivatives could substantially inhibit the proliferation of various types of cancer such as colon, breast and leukemia [13]. Recently, it has been found that piperazines containing compounds are likely to be more active and effective in treating cancer comparatively to the known

anticancer drugs such as taxane, sorafenib, cisplatin and doxorubicin and also, they are broadly prescribed as anticancer drugs [14]. Imatinib used for treating myelogenous leukemia consist of piperazine nucleus, thereby increasing its anticancer profile [15]. The anticancer activities of piperazine derivatives are due to their potential in inhibiting growth factors, enzymes and kinases possibly involved in the cellular immortality and carcinogenesis such as focal adhesion kinase (FAK) [16], insulin like growth factor-1 receptor (IGF-1R) [17] or to trigger oxidative stress causing mitochondrial impairment and apoptosis [18]. On the other hand, azetidin-2-one derivatives exhibits an extensive spectra of biological activities including antimicrobial, anti-tubercular, anti-cancer, anti-inflammatory, anti-malarial, etc. [19]. Chemical reactivity of azetidin-2-one ring which accounts for its enhanced biological profile is contributed by the substituted nitrogen atom and phenyl derivatives at C-4 position [20]. The anticancer activities of 2-azetidinones derivatives are related to their ability to inhibit proliferation either by inducing DNA damage [21], or by activating. Adenosine monophosphate activated protein kinase (AMPK) [19] and by bringing downstream PI3K/AKT/GSK-3 β (glycogen synthase kinase) signaling pathways [20]. Inducing apoptosis directly is an important characteristic feature of these azole derivatives which enables them in removing cancer cells effectively, thereby making them perfect candidate for cancer drug development. The aim of this study is to evaluate the anti-proliferative properties of piperazine/2-azetidinone derivatives against human cervical cancer cells and also to evaluate the effectiveness of these synthetic derivatives as apoptosis inducers (Fig. 1).

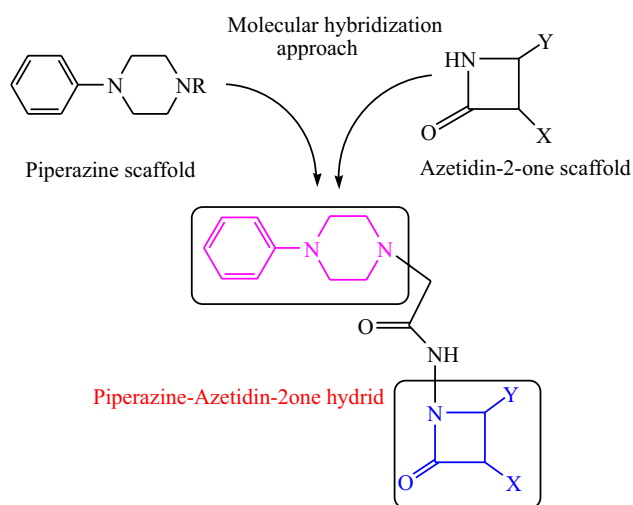


Fig. 1 General structure of piperazine clubbed with azetidin-2-one derivatives

Materials and methods

Chemistry

All the chemicals used in experiments were purchased from Sigma-Aldrich, Merck (Germany) and were employed without carrying any further purification. MEL-temp apparatus was employed to determine the melting points for all derivatives and results were uncorrected. For assessing the purity of compounds, CHN Elemental analyzer (Vario EL-III) was used and values so obtained were found to be within range of $\pm 0.3\%$ of the observed values. IR spectra for all synthetic compounds were taken on Bruker Tensor 37 FTIR spectrometer and wave numbers were calculated in cm^{-1} . NMR (^1H NMR and ^{13}C NMR) spectra were obtained using Bruker Advance 300 MHz spectrometer with DMSO- d_6 as solvent. The chemical shift (δ) values and coupling constant (J) were mentioned in parts per million (ppm) and hertz respectively along with reference residual peaks of CDCl_3 (δ 7.24, ^1H NMR; δ 77.0, ^{13}C NMR) or DMSO- d_6 (δ 2.49, ^1H NMR, δ 39.70, ^{13}C NMR). ESI-MS spectra were recorded on AB-Sciex 2000.

General protocol for synthesis of piperazine clubbed with 2-azetidinone derivatives (5a–5h)

To the solution of *N'*-(4-substitutedbenzylidene)-2-(4-phenylpiperazin-1-yl) acetohydrazide (**4a–4h**) (0.01 mol) in dioxane (10–15 ml), chloroacetylchloride (0.01 mol) and triethylamine (0.01 mol) was added carefully dropwise while maintaining the stirring at 0–5 °C. The reaction mixture was allowed to reflux for 24 h. The reaction mixture on completion was poured onto crushed ice which precipitates, filtered, and dried. The crude product so obtained was further purified through recrystallization using mixture of solvents (DCM/methanol).

***N*-(3-chloro-2-oxo-4-phenylazetidin-1-yl)-2-(4-phenylpiperazin-1-yl)acetamide (5a)** Yield: 64.6%; mp: 155–157 °C; Anal Calcd for $\text{C}_{21}\text{H}_{23}\text{ClN}_4\text{O}_2$: C, 63.23; H, 5.81; N, 14.05%; found C, 63.21; H, 5.80; N, 14.03%. IR (ν_{max} cm^{-1}): 3132, 3081 (Ar–H), 3093 (NH stretch), 1754 (2-azetidinone ring $\text{C}=\text{O}$), 1624 ($\text{C}=\text{O}$ of CONH), 1595, 1505 ($\text{C}=\text{C}$ aromatic), 1380 (C–N), 813 (C–Cl); ^1H NMR (DMSO- d_6) δ (ppm): 8.57 (s, 1H, CONH), 7.31 (s, 1H, phenyl ring), 7.20–7.16 (d, 2H, $J=6.6$ Hz, aromatic protons), 6.84–6.80 (d, 2H, $J=6.6$ Hz, aromatic protons), 7.52–7.42 (m, 5H, phenylpiperazine), 6.32 (s, 2H, NCH_2), 5.32 (s, 1H, CH–Ar, 2-azetidinone ring), 3.37–3.34 (q, 4H, CH_2NCH_2 , phenylpiperazine ring),

$J=6.7$ Hz), 2.75–2.73 (t, 4H, $-\text{CH}_2-\text{N}-\text{CH}_2$, phenylpiperazine ring, $J=6.67$ Hz), 2.45 (s, 1H, $\text{CH}-\text{Cl}$, 2-aetidione ring); $^{13}\text{CNMR}$ ($\text{DMSO}-d_6$) δ (ppm) 163.5, 152.67, 145.45, 128.88, 128.3, 126.7, 122.2, 119.68, 116.11, 70.3, 59.1, 49.75, 45.31; ESI-MS m/z : $[\text{M} + \text{H}]^+$ 399.89.

***N*-(3-chloro-2-(4-chlorophenyl)-4-oxazaetid-1-yl)-2-(4-phenylpiperazine-1-yl)acetamide (5b)** Yield: 66.7%; mp: 169–171 °C; Anal Calcd for $\text{C}_{21}\text{H}_{22}\text{Cl}_2\text{N}_4\text{O}_2$: C, 58.21; H, 5.12; N, 12.93% found C, 58.21; H, 5.10; N, 12.93% IR (ν_{max} cm^{-1}): 3100, 3018 (Ar–H), 3086 (NH stretch), 1752 (2-azetidione ring $\text{C}=\text{O}$), 1604 ($\text{C}=\text{O}$ of $-\text{CONH}$), 1593, 1515 ($\text{C}=\text{C}$ aromatic), 1387 (C–N), 780 (C–Cl); $^1\text{HNMR}$ ($\text{DMSO}-d_6$) δ (ppm): 8.53 (s, 1H, CONH), 7.18–7.14 (d, 2H, $J=6.6$ Hz), 6.82–6.78 (d, 2H, $J=6.7$ Hz), 7.51–7.41 (m, 4H, phenyl), 6.42 (s, 2H, $-\text{NCH}_2$), 5.43 (s, 1H, $\text{CH}-\text{Ar}$, 2-azetidione ring), 3.35–3.33 (q, 4H, $-\text{CH}_2-\text{N}-\text{CH}_2$, phenylpiperazine ring, $J=6.67$ Hz), 2.73–2.71 (t, 4H, $-\text{CH}_2-\text{N}-\text{CH}_2$, phenylpiperazine ring, $J=6.8$ Hz), 2.43 (s, 1H, $-\text{CH}-\text{Cl}$, 2-aetidione ring); $^{13}\text{CNMR}$ ($\text{DMSO}-d_6$) δ (ppm), 167.67, 155.17, 146.17, 129.98, 127.44, 125.7, 121.2, 117.83, 115.57, 74.43, 56.91, 45.85, 43.11; ESI-MS m/z : $[\text{M} + \text{H}]^+$ 434.33.

***N*-(3-chloro-2-(2-hydroxyphenyl)-4-oxoazetid-1-yl)-2-(4-phenylpiperazin-1-yl)acetamide (5c)** Yield: 54.16%; mp: 173–175 °C; Anal Calcd for $\text{C}_{21}\text{H}_{23}\text{ClN}_4\text{O}$: C, 60.79; H, 5.59; N, 13.50%; found C, 60.60; H, 5.57; N, 13.53%. IR (ν_{max} cm^{-1}): 3234, 3111 (Ar–H), 3102 (NH stretch), 1766 (azetidione ring $-\text{C}=\text{O}$), 1631 ($\text{C}=\text{O}$ of $-\text{CONH}$), 1605, 1515 ($\text{C}=\text{C}$ aromatic), 1399 (C–N), 781 (C–Cl); $^1\text{HNMR}$ ($\text{DMSO}-d_6$) δ (ppm): 10.31 (s, 1H), 8.34 (s, 1H, CONH), 7.56–7.44 (m, 4H), 7.71–7.67 (m, 5H, phenyl), 6.22 (s, 2H, $-\text{NCH}_2$), 5.22 (s, 1H, $\text{CH}-\text{Ar}$, 2-azetidione ring), 3.33–3.29 (q, 4H, $-\text{CH}_2-\text{N}-\text{CH}_2$, phenylpiperazine ring, $J=6.8$ Hz), 2.75–2.73 (t, 4H, phenylpiperazine ring $-\text{CH}_2-\text{N}-\text{CH}_2$, $J=6.66$ Hz), 2.42 (s, 1H, $-\text{CH}-\text{Cl}$, 2-aetidione ring); $^{13}\text{CNMR}$ ($\text{DMSO}-d_6$) δ (ppm): 165.37, 158.17, 155.15, 131.28, 129.27, 124.17, 120.12, 117.58, 114.91, 69.98, 61.1, 52.19, 43.21; ESI-MS m/z : $[\text{M} + \text{H}]^+$ 415.89.

***N*-(3-chloro-2-(2-methoxyphenyl)-4-oxoazetid-1-yl)-2-(4-phenylpiperazin-1-yl)acetamide (5d)** Yield: 57.66%; mp: 181–179 °C; Anal Calcd for $\text{C}_{22}\text{H}_{25}\text{ClN}_4\text{O}_3$: C, 61.61; H, 5.87; N, 13.06%; found C, 61.61; H, 5.83; N, 13.03%. IR (ν_{max} cm^{-1}): 3129, 3083 (Ar–H), 3091 (NH stretch), 1756 ($\text{C}=\text{O}$ of 2-azetidione ring), 1616 ($\text{C}=\text{O}$ of $-\text{CONH}$), 1593, 1502 ($\text{C}=\text{C}$ aromatic), 1382 (C–N), 815 (C–Cl); $^1\text{HNMR}$ ($\text{DMSO}-d_6$) δ (ppm): 9.66 (s, 1H, CONH), 8.33 (s, 3H, OCH_3), 7.51–7.41 (m, 5H, phenyl), 7.21–7.17 (m, 4H), 6.30 (s, 2H, CH_2), 5.31 (s, 1H, CH , $-\text{Ar}$, 2-azetidionering), 3.36–3.33 (q, 4H, $-\text{CH}_2-\text{N}-\text{CH}_2$, $J=6.81$ Hz, phenylpiperazine ring), 2.74–2.72 (t, 4H, $-\text{CH}_2-\text{N}-\text{CH}_2$,

$J=6.671$ Hz, phenylpiperazine ring), 2.43 (s, 1H, $-\text{CH}-\text{Cl}$, 2-aetidione ring); $^{13}\text{CNMR}$ ($\text{DMSO}-d_6$) δ (ppm): 161.5, 151.67, 143.40, 129.78, 128.29, 126.64, 121.47, 118.78, 116.01, 71.13, 60.21, 49.65, 45.21; ESI-MS m/z : $[\text{M} + \text{H}]^+$ 429.91.

***N*-(3-chloro-2-(3-nitrophenyl)-4-oxoazetid-1-yl)-2-(4-phenylpiperazin-1-yl)acetamide (5e)** Yield: 61.96%; mp: 163–165 °C; Anal Calcd for $\text{C}_{21}\text{H}_{22}\text{ClN}_5\text{O}_4$: C, 56.82; H, 5.00; N, 15.78%; found C, 56.80; H, 5.00; N, 15.76%. IR (ν_{max} cm^{-1}): 3330, 3181 (Ar–H), 2993 (NH stretch), 1734 ($\text{C}=\text{O}$ of 2-azetidione ring), 1614 ($\text{C}=\text{O}$ of $-\text{CONH}$), 1591, 1515 ($\text{C}=\text{C}$ aromatic), 1383 (C–N), 793 (C–Cl); $^1\text{HNMR}$ ($\text{DMSO}-d_6$) δ (ppm): 8.85 (s, 1H, CONH), 8.05 (s, 1H), 7.45–7.30 (m, 2H), 7.28–7.20 (m, 5H, phenyl), 6.26 (s, 2H, $-\text{NCH}_2$), 6.85–6.82 (d, 2H, $J=6.7$ Hz), 5.26 (s, 1H, $\text{CH}-\text{Ar}$, 2-azetidione ring), 3.33–3.30 (q, 4H, $-\text{CH}_2-\text{N}-\text{CH}_2$, $J=5.12$ Hz, phenylpiperazine ring), 2.66–2.64 (t, 4H, $-\text{CH}_2-\text{N}-\text{CH}_2$, $J=6.671$ Hz, phenylpiperazine ring) 2.51 (s, 1H, $-\text{CH}-\text{Cl}$, 2-aetidione ring); $^{13}\text{CNMR}$ ($\text{DMSO}-d_6$) δ (ppm): 167.62, 153.41, 141.36, 131.52, 130.99, 129.45, 128.82, 115.76, 110.95, 76.67, 62.91, 43.76, 41.91; ESI-MS m/z : $[\text{M} + \text{H}]^+$ 444.88.

***N*-(3-chloro-2-(2-nitrophenyl)-4-oxoazetid-1-yl)-2-(4-phenylpiperazin-1-yl)acetamide (5f)** Yield: 57.86%; mp: 158–161 °C; Anal Calcd for $\text{C}_{21}\text{H}_{22}\text{ClN}_5\text{O}_4$: C, 56.82; H, 5.00; N, 15.78% found C, 56.80; H, 5.00; N, 15.76%. IR (ν_{max} cm^{-1}): 3329, 3176 (Ar–H), 3112 (NH stretch), 1744 ($\text{C}=\text{O}$ of 2-azetidione ring), 1621 ($\text{C}=\text{O}$ of $-\text{CONH}$), 1592, 1505 ($\text{C}=\text{C}$ aromatic), 1380 (C–N), 813 (C–Cl); $^1\text{HNMR}$ ($\text{DMSO}-d_6$) δ (ppm): 8.76 (s, 1H, CONH), 7.64–7.57 (m, 4H), 6.82–6.79 (d, 2H, $J=6.8$ Hz), 7.50–7.40 (m, 5H, phenyl), 6.31 (s, 2H, $-\text{NCH}_2$), 5.22 (s, 1H, $\text{CH}-\text{Ar}$, 2-azetidione ring), 3.37–3.34 (q, 4H, $-\text{CH}_2-\text{N}-\text{CH}_2$, $J=6.8$ Hz, phenylpiperazine ring), 2.73–2.71 (t, 4H, $-\text{CH}_2-\text{N}-\text{CH}_2$, $J=6.67$ Hz, phenylpiperazine ring), 2.43 (s, 1H, $-\text{CH}-\text{Cl}$, 2-aetidione ring); $^{13}\text{CNMR}$ ($\text{DMSO}-d_6$) δ (ppm): 160.5, 150.67, 143.55, 129.79, 126.63, 125.67, 121.2, 117.78, 115.21, 70.54, 59.91, 49.75, 45.31; ESI-MS m/z : $[\text{M} + \text{H}]^+$ 444.88.

***N*-(3-chloro-2-(4-nitrophenyl)-4-oxoazetid-1-yl)-2-(4-phenylpiperazin-1-yl)acetamide (5g)** Yield: 54.16%; mp: 186–189 °C; Anal Calcd for $\text{C}_{21}\text{H}_{22}\text{ClN}_5\text{O}_4$: C, 56.82; H, 5.00; N, 15.78%; found C, 56.80; H, 5.00; N, 15.76%. IR (ν_{max} cm^{-1}): 3332, 3191 (Ar–H), 3100 (NH stretch), 1678 ($\text{C}=\text{O}$ of 2-azetidione ring), 1601 ($\text{C}=\text{O}$ of $-\text{CONH}$), 1587, 1554 ($\text{C}=\text{C}$ aromatic), 1288 (C–N), 767 (C–Cl); $^1\text{HNMR}$ ($\text{DMSO}-d_6$) δ (ppm): 9.03 (s, 1H, CONH), 7.60–7.56 (m, 2H), 6.74–6.70 (d, 2H, $J=6.8$ Hz), 7.43–7.33 (m, 5H, phenyl), 6.45 (s, 2H, $-\text{NCH}_2$), 5.72 (s, 1H, $\text{CH}-\text{Ar}$, 2-azetidione ring), 3.77–3.74 (q, 4H, $-\text{CH}_2-\text{N}-\text{CH}_2$, $J=6.67$ Hz, phenylpiperazine ring), 2.55–2.53 (t, 4H, $-\text{CH}_2-\text{N}-\text{CH}_2$,

$J=5.0$ Hz, phenylpiperazine ring), 2.66 (s, 1H, $-\text{CH}-\text{Cl}$, 2-aetidione ring); $^{13}\text{CNMR}$ (DMSO- d_6) δ (ppm): 162.68, 157.87, 143.58, 127.17, 122.73, 123.50, 120.96, 117.89, 114.71, 71.52, 52.81, 42.68, 40.71; ESI-MS m/z : $[\text{M}+\text{H}]^+$ 444.88.

***N*-(3-chloro-2-(4-aminophenyl)-4-oxoazetidin-1-yl)-2-(4-phenylpiperazin-1-yl)acetamide (5h)** Yield: 69.26%; mp: 177–179 °C; Anal Calcd for $\text{C}_{21}\text{H}_{24}\text{ClN}_5\text{O}_2$: C, 60.94; H, 5.84; N, 16.92%; found C, 60.91; H, 5.80; N, 16.93%. IR (ν_{max} cm^{-1}): 3131, 3085 (Ar-H), 3096 (NH stretch), 1752 (C=O of 2-azetidinone ring), 1622 (C=O of $-\text{CONH}$), 1592, 1515 (C=C aromatic), 1387 (C-N), 802 (C-Cl); $^1\text{HNMR}$ (DMSO- d_6) δ (ppm): 8.55 (s, 1H, CONH), 7.51–7.47 (d, 2H, $J=6.7$ Hz), 7.49–7.39 (m, 5H, phenyl), 7.23–7.19 (m, 2H), 6.31 (s, 2H, $-\text{NCH}_2$) 5.32 (s, 1H, CH-Ar, 2-azetidione ring), 5.01 (s, 2H, $-\text{NH}_2$), 3.41–3.39 (q, 4H, $-\text{CH}_2-\text{N}-\text{CH}_2$, $J=46.6$ Hz, phenylpiperazine ring), 2.66–2.65 (t, 4H, $-\text{CH}_2-\text{N}-\text{CH}_2$, $J=6.67$ Hz, phenylpiperazine ring), 2.58 (s, 1H, $-\text{CH}-\text{Cl}$, 2-aetidione ring); $^{13}\text{CNMR}$ (DMSO- d_6) δ (ppm): 167.34, 157.87, 140.91, 131.56, 130.99, 129.48, 128.83, 123.18, 123.10, 116.82, 113.517,

$$\% \text{ Inhibition} = \frac{\text{Mean OD of untreated cells (control)} - \text{mean OD of treated cells}}{\text{Mean OD of untreated cells (control)}} \times 100$$

74.83, 62.34, 46.95, 42.864, 40.62 ESI-MS m/z : $[\text{M}+\text{H}]^+$ 414.16.

Pharmacology

Antibodies and reagents

All chemicals including RPMI-1640, fetal bovine serum, trypsin and antibodies were brought from GIBCO Grand Island, New York, USA while reagents like bovine serum albumin (BSA), ethidium bromide (EtBr), acridine orange (AO), Triton X-100, and 3-(4,5-dimethylthiazol-2-yl)-2,5-diphenyl-tetrazolium bromide (MTT), JC-1 dye, propidium iodide (PI), RNase-A, proteinase-K were brought from Sigma-Aldrich, St. Louis, MO, USA. Primary mice β -actin, primary rabbit cytochrome-*c*, primary mice caspase-3 and secondary antimice Ig-G-HRP and antirabbit Ig-G-HRP antibodies were purchased from Santa Cruz Biotechnology, Texas, USA. All other important chemicals used were of molecular biology grade.

Cell culture

Human cervical cancer cell (HeLa) line was brought from National Center for Cell Science, Department of Biotechnology, Pune, India. Cells were incubated at 37 °C with 5% CO_2 in RPMI-1640 medium as monolayer supplemented with 10% (v/v) FBS, antibiotics (penicillin 100 U/ml, streptomycin 10 $\mu\text{g}/\text{ml}$) and 1 mmol/l sodium pyruvate solution.

Cell proliferation (MTT assay)

To evaluate the proliferation of HeLa cells, MTT assay was used. 96-well plate was used to seed cells having density of 5×10^3 cells/well and kept overnight for attachment. Media was replaced and cells were exposed for 24 h to different concentrations (12.5–100 $\mu\text{g}/\text{ml}$) of compounds (**5a–5h**). 20 μl containing 5 mg/ml of MTT was poured to each well 4 h before the incubation would complete. The media was changed and 200 μl of DMSO was added followed by incubation at room temperature for another 10 min. ELISA reader was used to observed absorbance at 595 nm. The % of inhibition was calculated using following formula [22]:

IC_{50} values were calculated for compounds from the curves by plotting % inhibition versus concentration of compounds.

Morphological changes

Cells in equal number 1×10^3 were seeded in 60 mm well plates followed by treatment with various concentration of compound (**5e**). Cell morphology was observed after 24 h by using microscope (Nikon Eclipse Ti-S, Tokyo, Japan).

Clonogenic assay

1×10^3 cells/well were seeded in six well plates. After incubating cells for 37 °C and replacing media twice in a week, cells were washed twice thoroughly with PBS (phosphate buffer saline) and were fixed for 10 min in a fixative solution. Cells were stained for 10 min using crystal violet solution and then colonies were observed through naked eyes.

Wound healing assay

1×10^3 cells/well was seeded equally in six well plates. After 80% confluence of cells growth, a scratch was made

using 200 μ l pipette tip in each well plate and exposed to various concentrations of compound (**5e**). The photographs of cell scratch were taken at 0 and 24 h by using microscope (Nikon Eclipse Ti-S, Tokyo, Japan) and the percentage of wound thickness was calculated as a ratio of percentage of wound thickness after 24 h to initial wound thickness.

Cell cycle distribution analysis

60 mm dish was used to seed HeLa cells, after which cells were left for attachment followed by cells treatment with compound **5e** for 24 h. Harvesting and centrifugation of cells at 400 \times g was done for 10 min. This step was followed by discarding and fixation of pellets with 70% ethanol. Further washing of cells were done using PBS. Cells were then stained with 500 μ l of PI solution and 25 μ l of RNAase and left for incubation in dark room for 30 min at 37 °C. Fluorescence emission of PI-DNA complex to quantified apoptotic cells was done using FACS Caliber instrument (Becton Dickinson, Franklin Lakes, NJ, and USA). Each sample taken for examination consists of 20,000 cells. The distribution pattern of DNA content was expressed as subG1, G1, S, and G2/M phases.

Annexin V-FITC/propidium iodide (AV/PI) staining assay

Annexin-V-FITC/propidium iodide staining kit was employed for analysis apoptosis. Six-well plate containing cells were exposed to different concentrations of compound **5e** for 24 h. Cells were harvested followed by washing using cold PBS resuspended in 100 μ l binding buffer and mixed for about 30 min at room temperature containing annexin V-FITC and PI. Cells were analyzed through flow cytometry.

Assessment of nuclear morphology of apoptotic cells by acridine orange/ethidium bromide (AO/EtBr)

The AO/EtBr dual staining assay was used to evaluate the apoptosis in HeLa cells. Cells were suspended in a mixture containing AO/EtBr dual staining solution in 1:1 ratio (1 mg/ml of AO in PBS + 1 mg/ml of EtBr in PBS) for 2 min. To visualize cells, fluorescence microscopy (Nikon ECLIPSE Ti-E, Tokyo, Japan) was used. Cells were differentiated on the basis of fluorescence emitted where live; apoptotic and necrotic cells were seen as green, orange and red respectively in merged image.

DNA fragmentation assay

After treating cells with compound **5e** for 24 h, cells were collected through trypsinization and centrifugation for

10 min at around 500 rpm. The supernatant was discarded and washing was done with cold PBS twice. 500 μ l DNA lysis buffer (20 mM EDTA, 10 mM Tris-HCl pH 8.0, 0.2% Triton X-100 and 100 μ g/ml proteinase-K) was used for lysing the cells pellet at 37 °C for 1.5 h. To get the supernatant containing DNA, the samples were subjected to centrifugation for 5 min at 6000 \times g. To equal volume of isopropanol, the supernatant was added and 25 μ l 4M NaCl making a final concentration upto 100 mM and left for overnight incubation at -20 °C. Sample at room temperature was centrifuged at 6000 \times g for 25 min. A solution of 50 μ l double distilled water and 2 μ l RNase A (10 mg/ml) was used to dissolve the pellets and left for incubation for 1 h at 37 °C. Spectrophotometer, NanoDrop (NanoDrop, Wilmington, USA) was used to quantify the extracted DNA. 2% agarose gel containing 1 μ g/1 ml EtBr was used to electrophorese the DNA samples. The gel was examined and ultraviolet gel documentation system was used to take images.

Generation of intracellular reactive oxygen species (ROS)

Production of intracellular ROS (reactive oxygen species) in HeLa cells was measured using 2',7'-dichlorofluorescein diacetate (DCFHDA) dye. Cells with density of 5 \times 10⁵ cell/well were seeded over cover-slip of six-plated well and kept overnight for incubation for the attachment. Next day, cells were exposed to fresh media having different concentrations of compound (**5e**). Incubation of cells for 4 h at 37 °C was done. Then cells were stained with 40 μ M DCFHDA for 30 min. Cover slip was adhered on glass slide and fluorescence microscope (Nikon Eclipse Ti-E, Tokyo, Japan) was used for observe the results..

Assessment of mitochondrial membrane potential

To access the loss of the mitochondrial membrane potential, fluoroprobe 5,5',6,6'-tetrachloro-1,1',3,3'-tetraethylbenzimidazol-carbocyanine iodide (JC-1 dye) has been used extensively. Six-well plate was used for growing cells followed by exposure to various concentrations of compound (**5e**). After treating cells for 4 h, washing was done using PBS followed by staining cells with 2 μ g/ml of JC-1 dye and left for incubation for 30 min in dark at 37 °C. Cells were washed thoroughly with PBS (phosphate buffer saline) and live imaging microscope was used for capturing images. Fluorimeter was also used for measuring the mitochondrial membrane potential which requires treatment of cells with various concentration of compound **5e**. Cells were incubated at 37 °C for 4 h which were then stained for 20 min with the mitochondrial-membrane-permeable dye JC-1 (10 μ g/ml in PBS) at 37 °C. Following this, harvesting and washing with phosphate buffer saline was done and measurements were taken 530/590 nm.

Protein extraction and western blot analysis

100 mm plate was used for seeding the cells in equal number. After 80% cells confluent, cells were exposed for 24 h to various concentration of compound (**5e**). Cells were trypsinized and washed with PBS. Radio immuno precipitation assay (RIPA) buffer was used for extracting and estimating protein and protein concentration respectively. The protein was separated in 8% SDS-PAGE gel and was transferred to nitrocellulose membrane. Obstruction of membrane was done using 5% BSA in PBS. It was then probed with primary antibody and incubated with a secondary antibody conjugated using horseradish peroxidase (HRP). ECL kit was used to detect the bands and images were permanently captured in X-ray films. Results were analyzed with respect to loading control (β -actin).

Cytochrome c in cytosolic fraction

4 °C was maintained to carry all steps. After treating with compound **5e**, cells were trypsinized and washed with PBS and resuspended into 500 μ l fractionation buffer [Buffer HEPES (pH 7.4) 20 mM, KCl 10 mM, MgCl₂ 2 mM, EDTA 1 mM, EGTA 1 mM, DTT 1 mM protease inhibitors cocktail-50 μ l/10 ml buffer] and left for incubation for 15 min over ice. 1 ml syringe was used to pass cells suspension through a 27 gauge needle 10–15 times and left on ice for further 20 min and centrifuged at 720 \times g (3000 rpm) for 5 min Supernatant was collected and again centrifuged at 8000 rpm (10,000 \times g) for 5 min. Pellet was discarded and supernatant was used to study cytochrome-*c* in cytosolic fraction. Bradford dye was used to estimate protein concentration in cytosolic fraction. The extracted protein was separated in 8% SDS-PAGE gel for western blotting analysis.

Data analysis

All the data was represented as a mean \pm SD for three sets of independent experiments and value of significant (p values) were evaluated using an unpaired student's *t* test using the GraphPad Prism version 7.0 software (San Diego, CA, USA) and p values < 0.05 were considered to be statistically relevant.

Results

Chemistry

Synthesis of all compounds was carried out using simple and feasible chemical reactions as shown in Scheme 1. The initial reactant (**1**) used in the synthesis of key intermediate hydrazide (**3**) was purchased from Sigma and was employed

after carrying out purification through recrystallization. Ethyl-2-(4-phenylpiperazin-1-yl) acetate (**2**) and 2-(4-phenylpiperazin-1-yl) acetohydrazide (**3**) were synthesized using to reported protocol [23]. The reaction between acetohydrazine derivatives (**3**) with various aromatic aldehydes using ethanol as solvent to give Schiff base (**4a–4h**) was done using reported procedure [24]. Synthesis of final compounds (**5a–5h**) was carried out using Staudinger reaction which involves cyclization between substituted acetic acid acids or acid chlorides and imines in presence of base [25]. All synthesized compounds were obtained in yield of about 55–75% and were purified using Column chromatography hexane/ethylacetate in ratio of (7:3) as eluting medium. All the synthesized compounds were shown to in accordance with the spectroscopic data obtained from FT-IR, ¹HNMR, ¹³C NMR, ESI MS and CHN analysis (Figs. S.1, S.2, S.3 and S.4).

Pharmacology

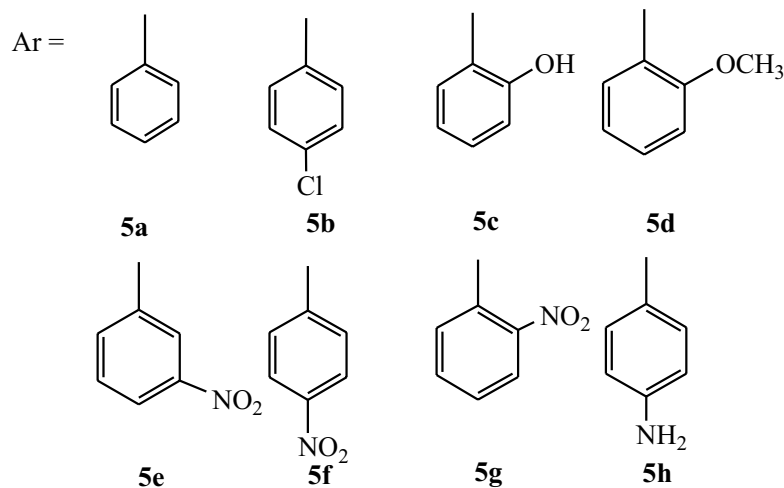
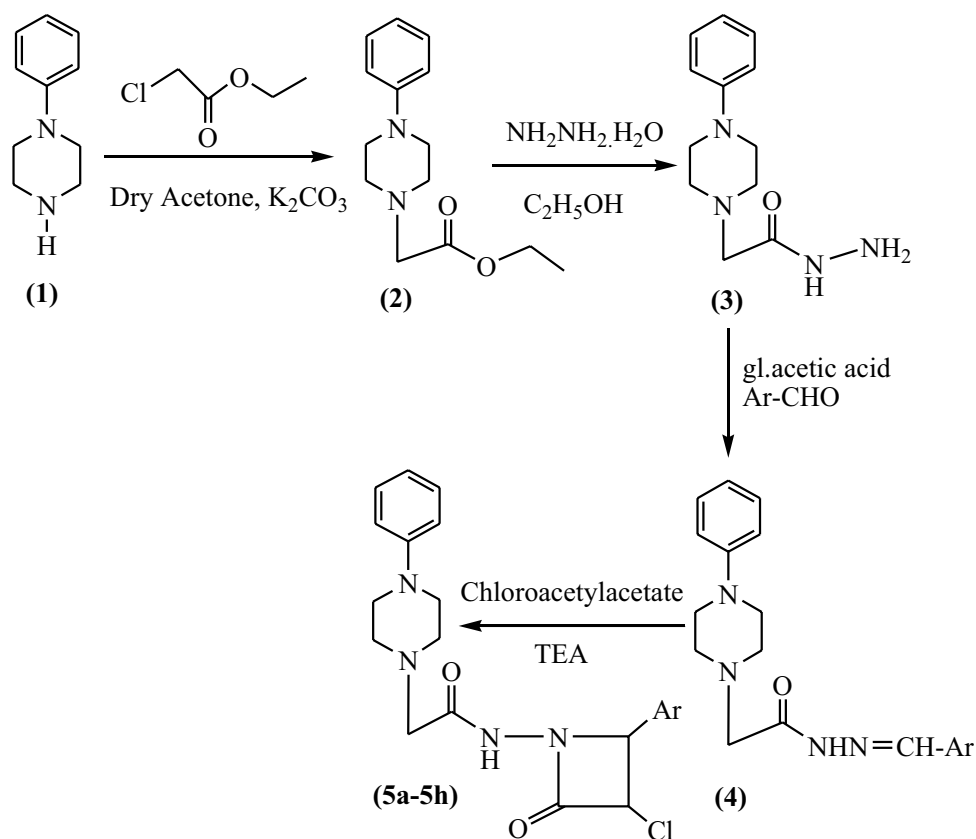
In vitro inhibition of cell growth by *N*-(3-chloro-2-(3-nitrophenyl)-4-oxoazetidin-1-yl)-2-(4-phenylpiperazin-1-yl) acetamide (**5e**)

The anti-proliferative effect of newly synthesized *N*-(3-chloro-2-(4-aryl)-4-oxoazetidin-1-yl)-2-(4-phenylpiperazin-1-yl) acetamide derivatives (**5a–5h**) on human cervical cancer cell line (HeLa) has been evaluated by MTT assay (Table 1). The cells were treated with final compounds (**5a–5h**) along with standard anticancer drug **5-Fluorouracil** in the concentration range of 12.5–100 μ g/ml for 24 h. Among all, compounds **5e** showed the highest inhibition towards HeLa cells with IC₅₀ value 29.44 \pm 1.46 μ g/ml in comparison to the reference anticancer drug **5-Fluorouracil** which exhibited less toxicity towards HeLa cells with very high IC₅₀ value 112.16 \pm 0.02 μ g/ml. Compound **5h** also showed moderate activity having IC₅₀ value 61.69 \pm 0.08 μ g/ml, while other compounds of the series were found to be inactive as they did not showed any activity upto 100 μ g/ml (Fig. S.5).

Evaluation for drug likeness properties of synthesized compounds

All the synthesized compounds were evaluated for some molecular properties based on Lipinski's rule of five which are physically and pharmaceutically significant. All the synthesized compounds exhibited optimum drug likeness properties without violating Lipinski's rule of five (Table 2) [26].

Scheme 1 Synthesis of piperazine clubbed 2-azetidine derivatives (**5a–5h**)



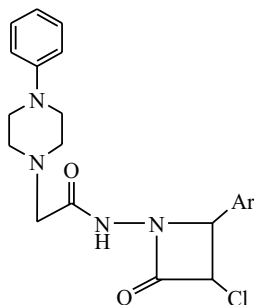
Morphological changes of HeLa cells induced by *N*-(3-chloro-2-(3-nitrophenyl)-4-oxoazetidin-1-yl)-2-(4-phenylpiperazin-1-yl)acetamide (**5e**)

Compound **5e** induced morphological changes in HeLa cells treated for 24 h in concentration dependent manner. The treated cells showed various morphological changes such as cell shrinkage, detachments and dead cells formation

whereas, untreated cells (control) appeared to be healthy in nature with normal shape and size (Fig. 2).

Decreased in number of HeLa cells in clonogenic assay by *N*-(3-chloro-2-(3-nitrophenyl)-4-oxoazetidin-1-yl)-2-(4-phenylpiperazin-1-yl)acetamide (**5e**)

Besides the effect of compound **5e** on cell viability and morphology, the number and size of cells were also evaluated

Table 1 Anti-proliferative activity of piperazine clubbed 2-azetidinone derivatives (**5a–5h**)

Compound no.	Ar group	HeLa
		IC ₅₀ (μg/ml) ± SD
5a		> 100
5b		> 100
5c		> 100
5d		> 100
5e		29.44 ± 1.46
5f		> 100
5g		> 100
5h		61.69 ± 0.08
5-Fluorouracil		112.16 ± 0.02

Bold values represent the IC₅₀ values of active compounds

No activity > 100 μM. The values (in μg/ml) represent the mean ± SE of three independent experiments. IC₅₀ is the concentration required to inhibit 50% of the cell population

HeLa human cervical cancer cell line

Table 2 Molecular properties of compounds

Compounds no.	Mi logp	TPSA	No. of atoms	MW	nON	nOHNH	Volume	Nrotb
Desirable value	<5	<140	–	<500	<10	<5	–	<10
5a	2.40	55.88	28	398.89	6	1	353.69	3
5b	3.08	55.88	29	433.34	6	1	367.20	5
5c	1.92	76.11	29	414.89	7	2	414.89	5
5d	2.46	65.12	30	428.92	7	1	379.24	6
5e	2.33	101.7	31	443.89	9	1	377.02	6
5f	2.36	101.7	31	443.89	9	1	377.02	6
5g	2.36	101.7	31	443.89	9	1	377.02	6
5h	1.48	81.91	29	413.91	7	3	364.98	5

MW molecular weight, *nviolations* number of violations, *natoms* number of atoms, *nON* number of hydrogen bond acceptors, *nOHNH* number of hydrogen bond donors, *Nrotb* number of rotatable bonds, *mi logp* logp value predicted by Molinspiration, *TPSA* topological polar surface area, *MV* molecular volume

using clonogenic assay. A cluster of approximately least 50 cells constitutes a colony. The clonogenic assay showed that the number and size of colonies significantly decreased when treated with compound **5e** in a concentration dependent manner in comparison to the untreated (control) cells which proliferated to form colonies (Fig. 3).

Inhibition of migration of HeLa cells by *N*-(3-chloro-2-(3-nitrophenyl)-4-oxoazetidin-1-yl)-2-(4-phenylpiperazin-1-yl)acetamide (**5e**)

In order to perform the in vitro cell migration assay wound was created on a confluent monolayer of cultured HeLa cells and exposed to different concentrations of **5e** (i.e. 12.5, 25

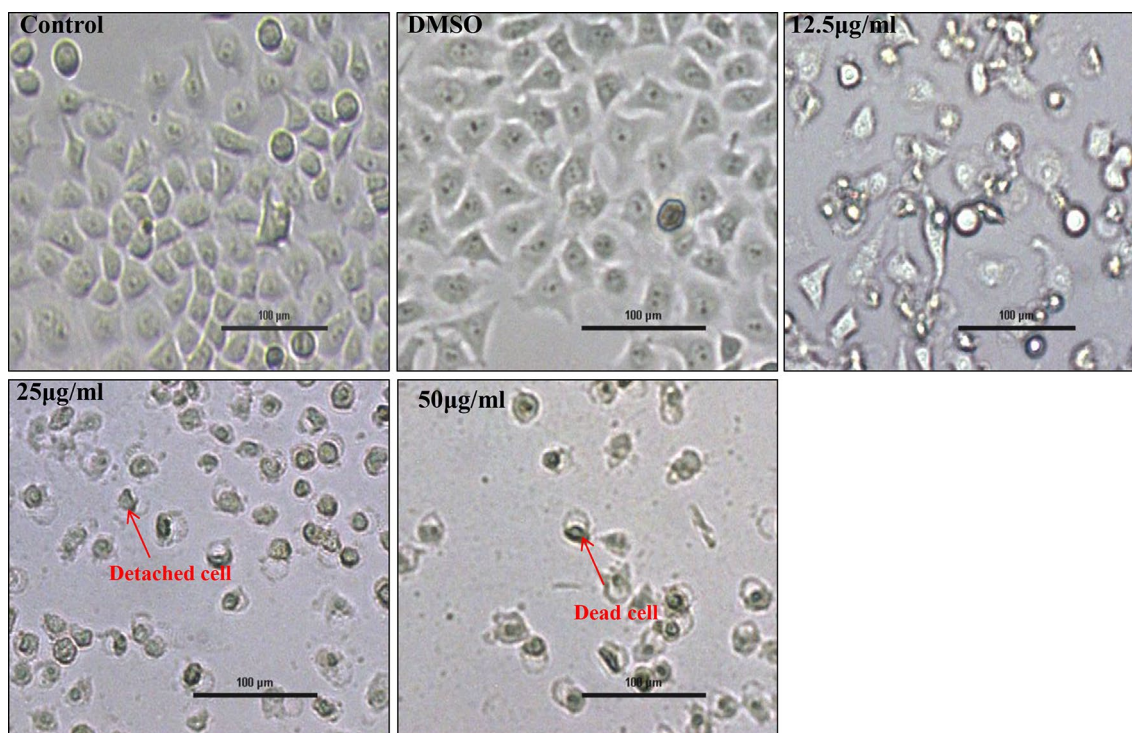
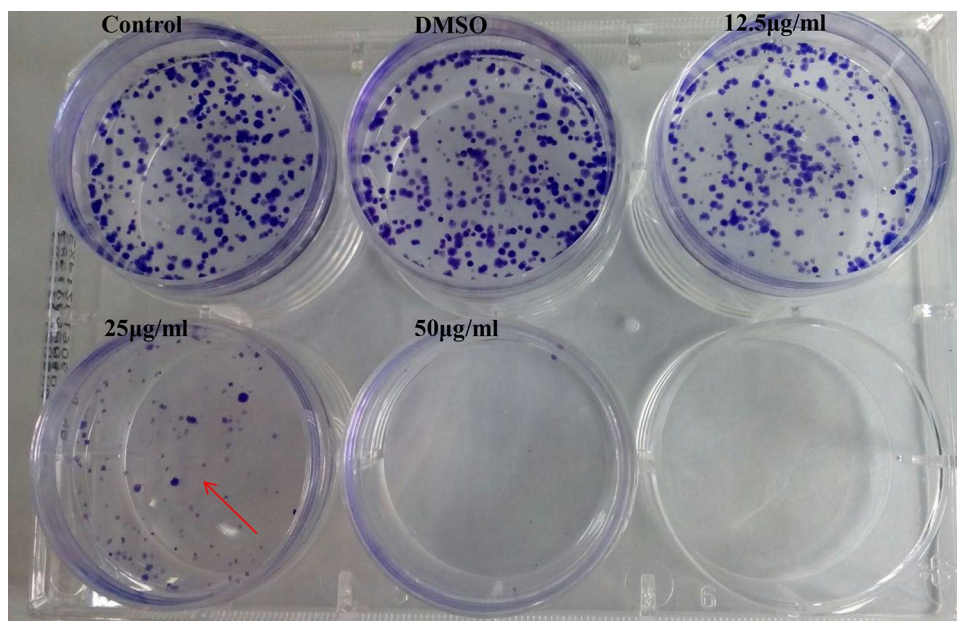


Fig. 2 Morphological changes such as detachments and dead cells were observed in HeLa cells treated for 24 h with compound **5e** in concentration dependent manner. (Images were captured using Nikon ECLIPSE Ti-S microscope at $\times 10$ magnification)

Fig. 3 Clonogenic assay (crystal violet staining) (arrow representing decrease in number and size of colonies in HeLa cells treated for 24 h with compound **5e** in concentration dependent manner)



and 50 $\mu\text{g/ml}$). The result showed that after 24 h, the thickness of wound gap decreased considerably for the untreated cells (control) cells in comparison with treated cells. The result showed that for treated cells the wound gap increased due to inhibition of migration of cells by compound **5e** in

concentration dependent manner (Fig. 4a). The percentage of wound thickness was found to be increasing from 56.81% (control) to 57.94% (solvent DMSO), 64.02% (12.5 $\mu\text{g/ml}$), 76.66% (25 $\mu\text{g/ml}$) and 92.8% (50 $\mu\text{g/ml}$) respectively (Fig. 4b), thus signifying the compound **5e** effectively

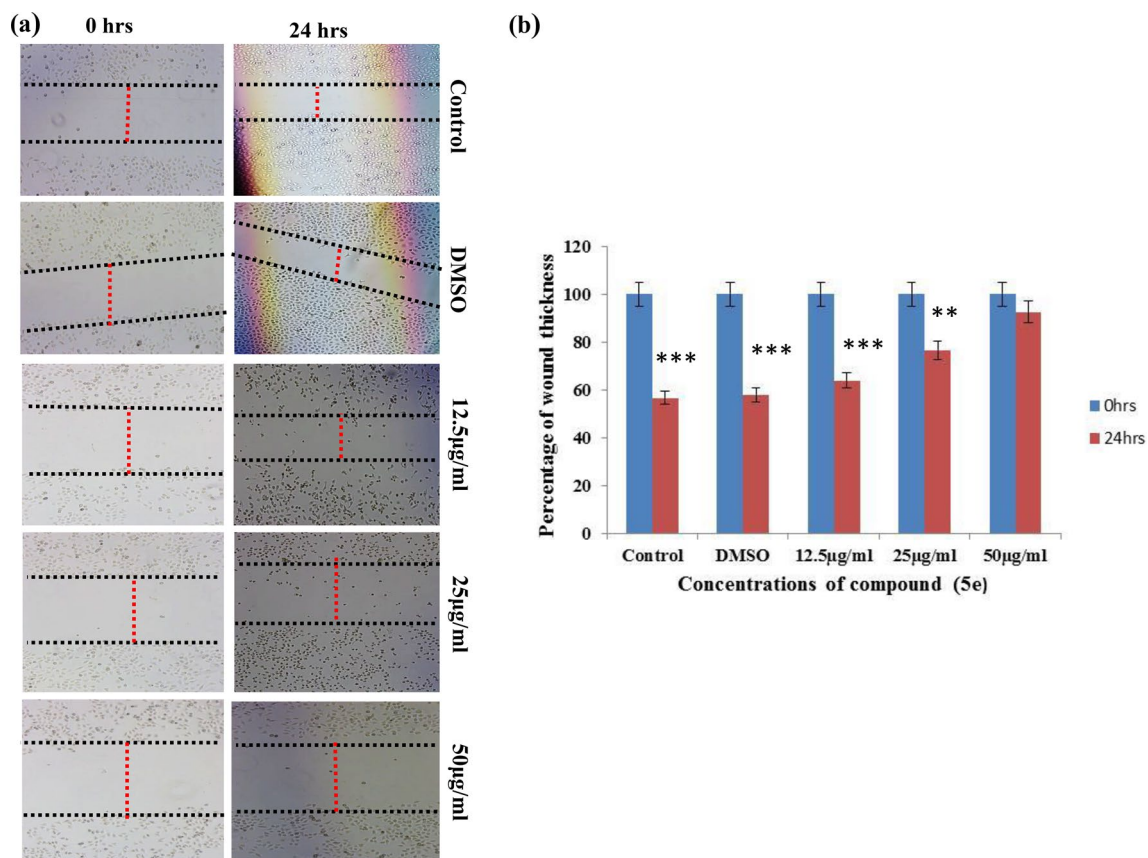


Fig. 4 **a** Wound-healing assay showed that **5e** inhibited the migration of HeLa cells. The photographs of cell scratch were taken using microscope (Nikon ECLIPSE Ti-S) at 0 and 24 h. **b** Relative

percentage of thickness of wound quantified using Graphpad prism 7. Data are presented as mean \pm SD of three separate experiment **** $p < 0.0001$, *** $p < 0.001$ with respect to control

suppressed the migration of HeLa cells in a concentration dependent manner.

***N*-(3-chloro-2-(3-nitrophenyl)-4-oxoazetidin-1-yl)-2-(4-phenylpiperazin-1-yl)acetamide (5e) induced G₂/M cell cycle arrest and apoptosis in HeLa cells**

Flow cytometric analysis of PI-stained cells showed that after 24 h treatment, the ratio of HeLa cells increased in the G₂/M phase ($p < 0.05$) from 11.51% (control) to 11.54% (DMSO), 13.06, 26.92 and 34.86% at 12.5, 25 and 50 μ g/ml concentrations of compound **5e** respectively (Fig. 5a). Concurrently, a noteworthy reduction ($p < 0.05$) in the population of HeLa cells in Sub-G₁ phase was observed. These results clearly indicated that compound **5e** led to apoptosis by arresting G₂/M phase of cell cycle (Fig. 5b). To further evaluate apoptosis induced by compound **5e**, we analyzed the disturbances in symmetry of plasma membrane, nuclear morphological changes and internucleosomal DNA fragmentation. Flow cytometry was employed to quantify the externalization

of phosphatidylserine (PS) in cell membrane of HeLa cells using annexin-V/propidium (AV/PI) dual staining dye. The result showed increase in the total percentage of apoptotic cells (early and late stage) and dead cells from (control) 8.87–9.28% (DMSO), (17.95)% 12.5 μ g/ml, (34.14)% 25 μ g/ml and (95.23)% 50 μ g/ml concentrations of compound **5e** respectively (Fig. 5c). The significant increase in total percentage of apoptotic cells (early and late) from 7.87% (control) to 8.31% (DMSO), 16.67% (12.5 μ g/ml), 32.98% (25 μ g/ml) and 94.68% (50 μ g/ml) in a concentration-dependent manner clearly showed that the compound **5e** induced apoptosis in HeLa cells (Fig. 5d). Concomitantly, compound **5e** induced apoptosis was further shown by change in membrane integrity and morphology of nucleus. AO/EtBr fluorescent staining assay differentiates the live, apoptotic and dead cells. The results showed that after 24 h, untreated cells (control) exhibited nuclei with normal morphology having intact membrane, uniform chromatin and appeared green in color, conversely nucleus of the AO/EtBr stained cells treated with different concentrations of compound **5e**, showed all three (green,

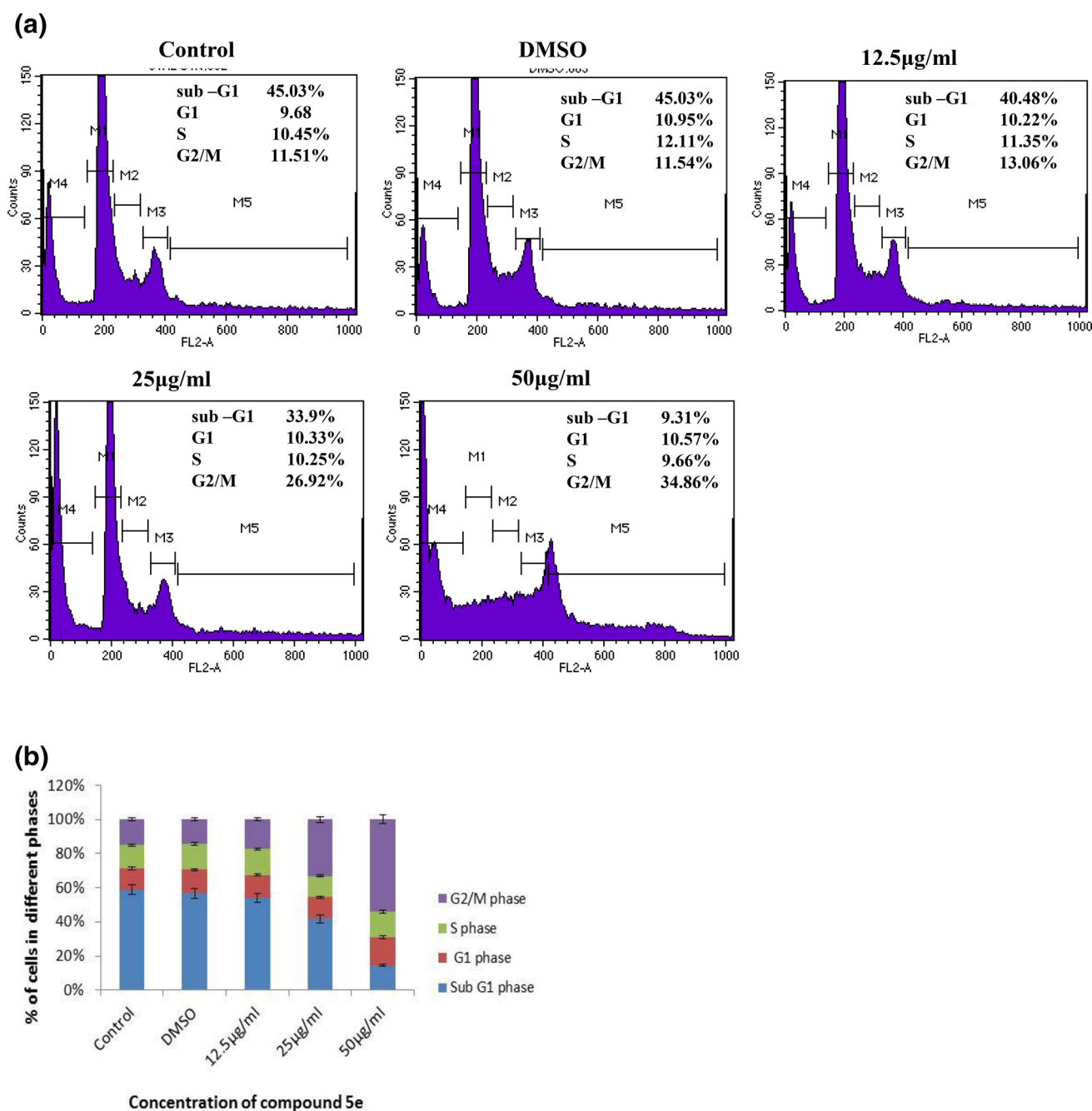


Fig. 5 **a** Cell cycle analysis of HeLa cells treated with different concentrations of **5e** for 24 h. The cell cycle distribution was performed by using propidium iodide staining and analyzed by flow cytometry BD FACS CALIBUR 4C. **b** Histogram of cell cycle distribution (%) in HeLa cells treated with different concentrations of **5e** for 24 h. Values are expressed as means \pm SD of three different experiments with $p < 0.05$. **c** Flow cytometry analysis of apoptosis induced by compound **5e** in HeLa cells treated in concentration dependent manner using through annexin V/PI staining quadrants; lower left (AV/PI-ve)-viable cells; upper right (AV/PI+ve)—late apoptosis; lower right (AV+ve)—early apoptosis and upper left (PI+ve)—second-

ary necrotic cells. **d** Increase in the population of apoptotic cells (early and late) with respect to different concentrations of compound **5e** after 24 h in HeLa cells. **e** Compound **5e** induced nuclear morphological changes in HeLa cells treated in concentration dependent manner related to apoptosis analyzed using EtBr/AO/staining. Green, orange and red fluorescence corresponds to live, apoptotic and dead cells respectively. Images were captured by fluorescence microscope (Nikon ECLIPSE TiE) at $\times 10$ magnification. **f** Effect of **5e** compound on HeLa cells by DNA ladder assay 24 h post treatment: 2% agarose gel showing the cleavage of HeLa cells genomic DNA (control) intact bands; (compound **5e**, 12.5, 25, 50 μ g/ml) forming DNA ladders

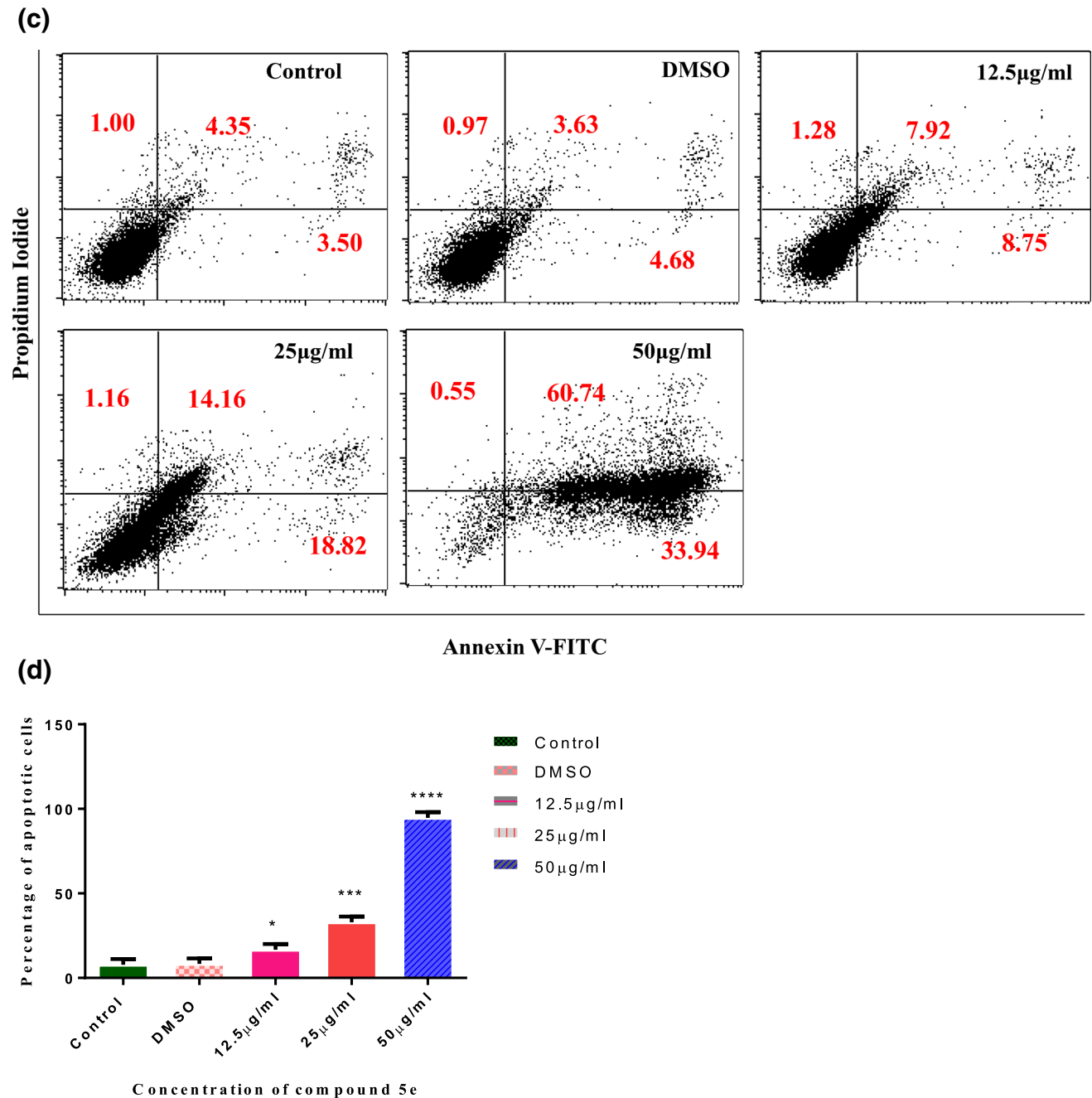


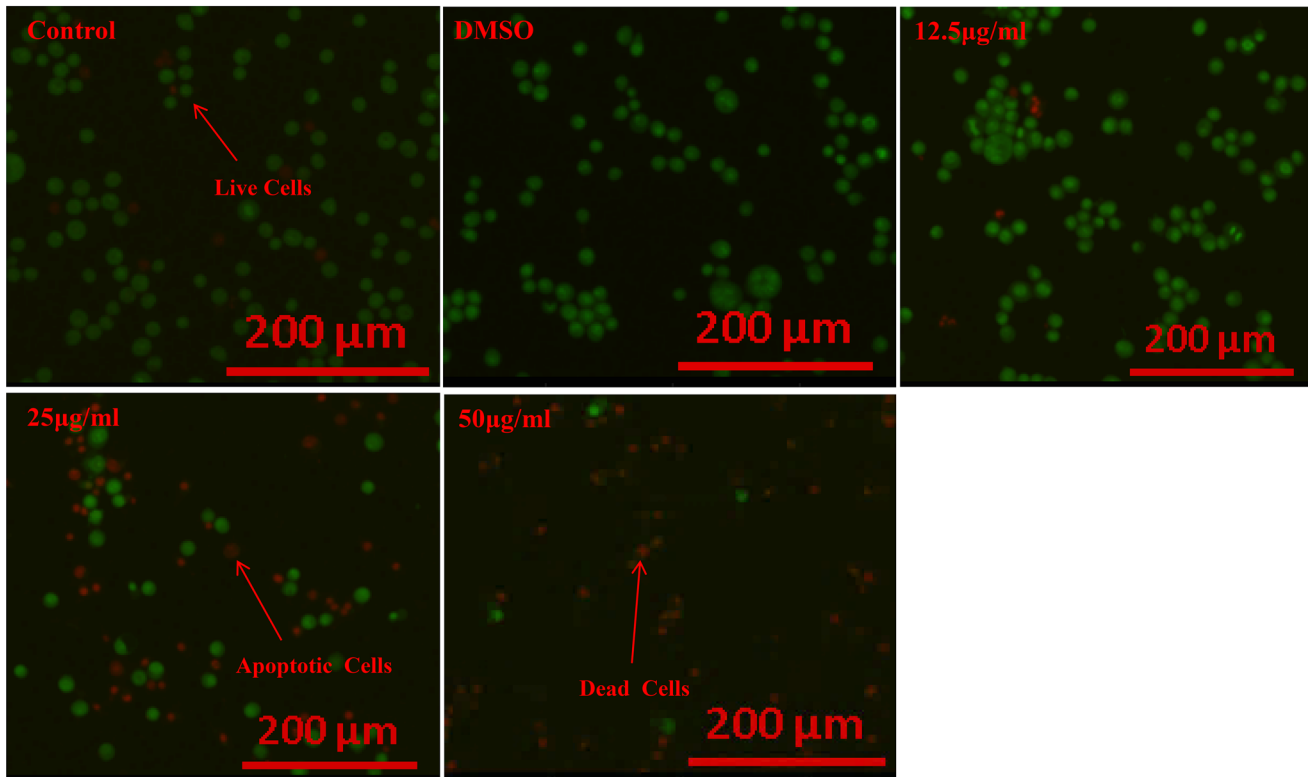
Fig. 5 (continued)

orange and red) fluorescence representing definitive damage of cell membrane (Fig. 5e). Further, DNA fragmentation was evaluated using gel electrophoresis. DNA ladder assay showed an intact DNA bands in untreated cells (control), while treated cells showed deteriorated bands forming ladder pattern in concentration dependent manner (Fig. 5f).

Generation of intracellular ROS levels using DCFH-DA assay by *N*-(3-chloro-2-(3-nitrophenyl)-4-oxoazetidin-1-yl)-2-(4-phenylpiperazin-1-yl)acetamide (5e)

To explore whether ROS played a prominent role in 5e-induced apoptosis, we used a fluorescent probe DCFH-DA to analyze the generation of cellular ROS in HeLa cells. The intensity of green fluorescence corresponds to the level of ROS produced in the cells. It was observed

(e)



(f)

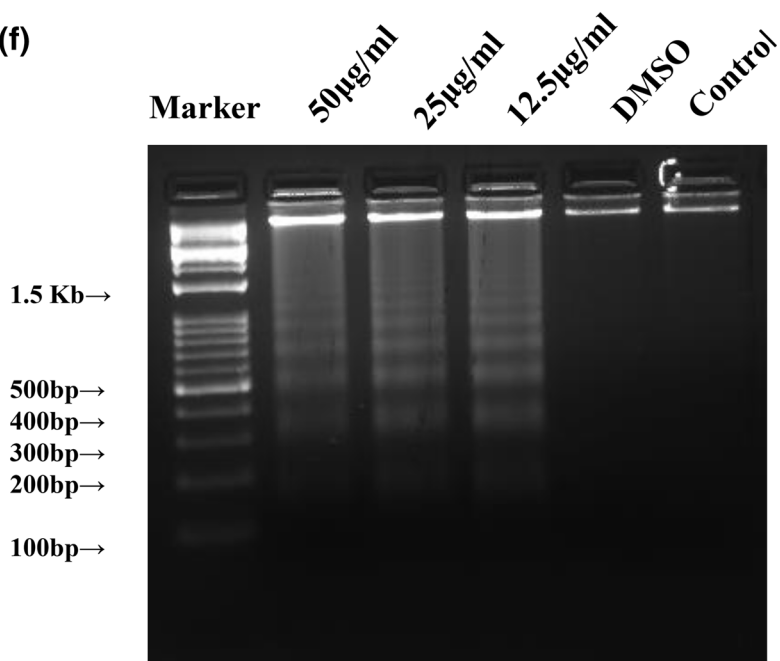


Fig. 5 (continued)

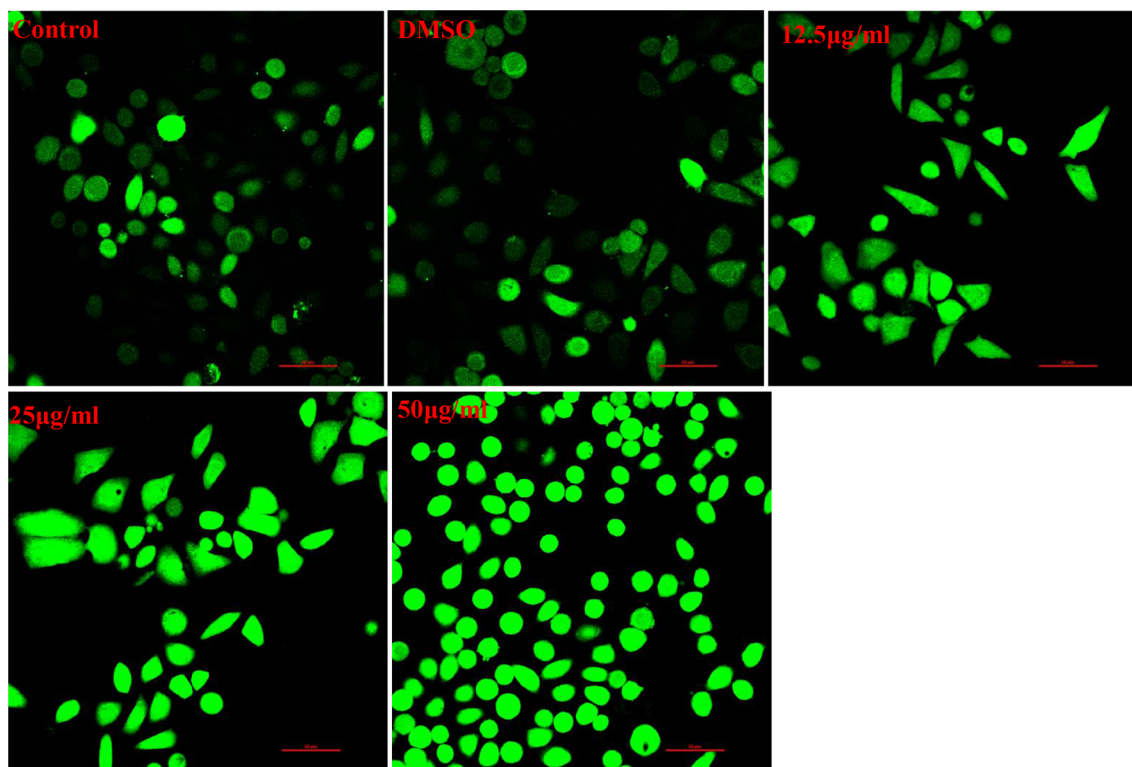


Fig. 6 Effect of different concentrations of **5e** on ROS level in HeLa cells after 6 h. Mark increased fluorescence with increasing concentration of compound **5e**. Images were captured by fluorescence microscope (Nikon ECLPSE Ti-E) at $\times 20$ magnification

clearly that after 24 h, the compound **5e** significantly increased the intensity of fluorescence in a concentration-dependent manner in HeLa cells, whereas control cells showed only a weak and diffused green fluorescence (Fig. 6).

Loss of mitochondrial membrane potential ($\Delta\Psi_m$) using JC-1 dye cell growth by *N*-(3-chloro-2-(3-nitrophenyl)-4-oxoazetidin-1-yl)-2-(4-phenylpiperazin-1-yl)acetamide (**5e**)

Mitochondrial membrane gets depolarized on loss of $\Delta\Psi_m$ damaging the mitochondrial functions and resulting in cell death. Variations in mitochondrial membrane potential was evaluated using JC-1 dye, as it forms red fluorescent aggregates in mitochondria corresponding to high membrane potential, whereas it forms green fluorescent monomers predominantly in cytosolic form, representing a collapse of membrane. As shown in (Fig. 7a), after 24 h, cells treated with different concentrations of compound **5e** exhibited strong green fluorescence in comparison to untreated (control) cells which displayed high red fluorescence. The results from (Fig. 7b) showed the decrease in percentage of $\Delta\Psi_m$

from 100% (control) to 81.69, 77.84 and 73.09% at 12.5, 25 and 50 $\mu\text{g/ml}$ concentrations of **5e** respectively.

Release of cytochrome *c* and activation of caspase-3 using western blotting by *N*-(3-chloro-2-(3-nitrophenyl)-4-oxoazetidin-1-yl)-2-(4-phenylpiperazin-1-yl)acetamide (**5e**)

The depolarization of mitochondrial membrane potential generally occurs before or in combination with release of cytochrome *c* from mitochondria to cytosol, which is one of the important processes that occur before apoptosis. In this regard, we have measured the expression of cytosolic cytochrome *c* in HeLa cells after exposed to different concentrations of compound **5e**. The western blot results showed elevation in the level of cytochrome *c* in the cytosol fraction (Fig. 8a). The translocation of cytochrome *c* from the mitochondria into cytosol ultimately results in apoptosis through activation of caspases. The results also showed that the compound **5e** significantly increased the activity of caspase-3 in concentration dependent manner (Fig. 8a). The change in the protein fold was analyzed using Image J software (Fig. 8b). All these results collectively showed that compound **5e** induce apoptosis in HeLa cells by the generation of cellular ROS through the intrinsic mitochondrial mediated apoptotic pathway (Fig. 9).

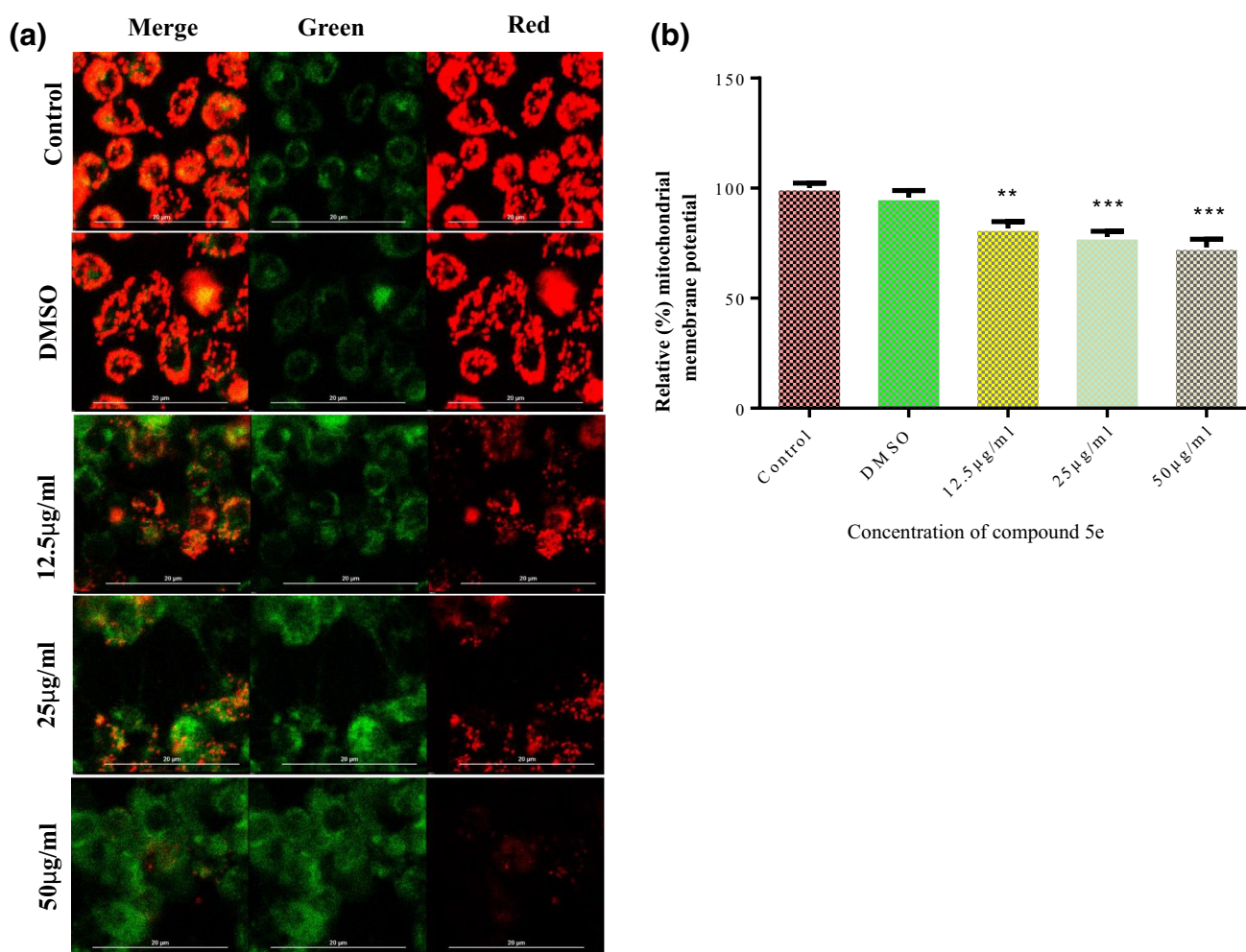


Fig. 7 **a** JC-1 staining representing the mitochondrial membrane depolarization of HeLa cells exposed to different concentrations of **5e** after 8 h: image were captured by live imaging microscope (Nikon ECLIPSE Ti) at $\times 20$ magnification. **b** Effect of **5e** on the loss of

mitochondrial membrane potential ($\Delta\Psi_m$) of HeLa cells using JC-1 dye: fluorescence was measured at 530/590 nm. Results are presented as mean \pm SD of triplicates ** $p < 0.01$, *** $p < 0.001$, with respect to control

Discussion

In the current study, a new series of *N*-phenylpiperazines containing 2-azetidinones derivatives were synthesized, characterized using high resolution spectroscopic techniques such as FT-IR, ^1H NMR, ^{13}C NMR, ESI-MS and CHN analysis and evaluated for their anti-proliferative effects on (HeLa) human cervical cancer cell line using MTT assay [27]. **5-Fluorouracil** was taken as a standard drug for assay. The IC_{50} values ($\mu\text{g}/\text{ml}$) for both synthesized compounds (**5a–5h**) and standard drug (**5-Fluorouracil**) were represented in Table 1. The in-vitro cytotoxic studies show that out of all, only two compounds **5e** and **5h** significantly inhibits the growth of human cervical cancer cell line (HeLa) in a concentration dependent manner.

MTT results show that the anti-proliferating property of the synthesized compounds is due to the variations and

modifications within structural framework. The substituents present on the phenyl ring on 2-azetidinone ring are important in analyzing structure–activity relationship (SAR) (Scheme 1). Compounds with unsubstituted phenyl ring (**5a**) were found to be less active and effective towards HeLa cancer cells in comparison with the substituted phenyl ring (**5b–5h**). It was observed that phenyl ring substituted with strong electron donating group ($-\text{NH}_2$) (**5h**) at para position and strong electron withdrawing group ($-\text{NO}_2$) (**5e**) at meta position respectively showed higher activity than the standard drug (**5-Fluorouracil**) towards HeLa cancer cells in concentration dependent treatment. Phenyl ring having ortho substitution with either strong or weak electron withdrawing or donating group showed no activity (**5b–5d**, **5f**). Among all, compound **5e** show highest inhibitory effect with IC_{50} value of $29.44 \pm 1.46 \mu\text{g}/\text{ml}$ on HeLa cells. The significant anti-proliferative effect of compound **5e** towards HeLa

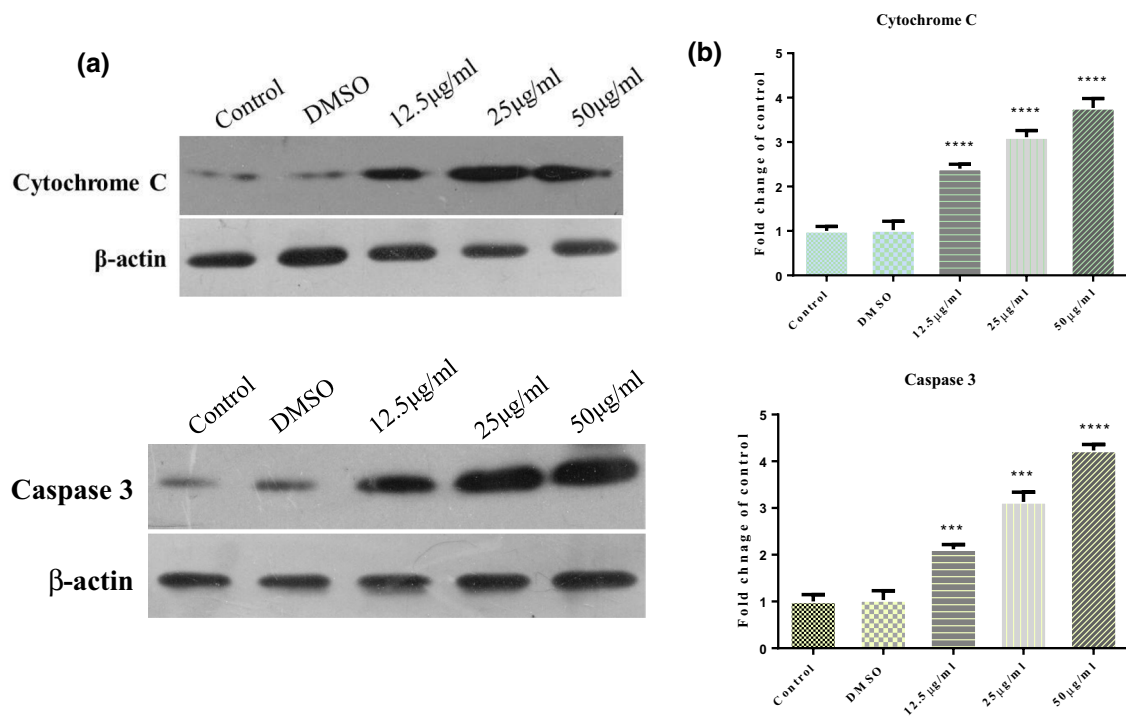
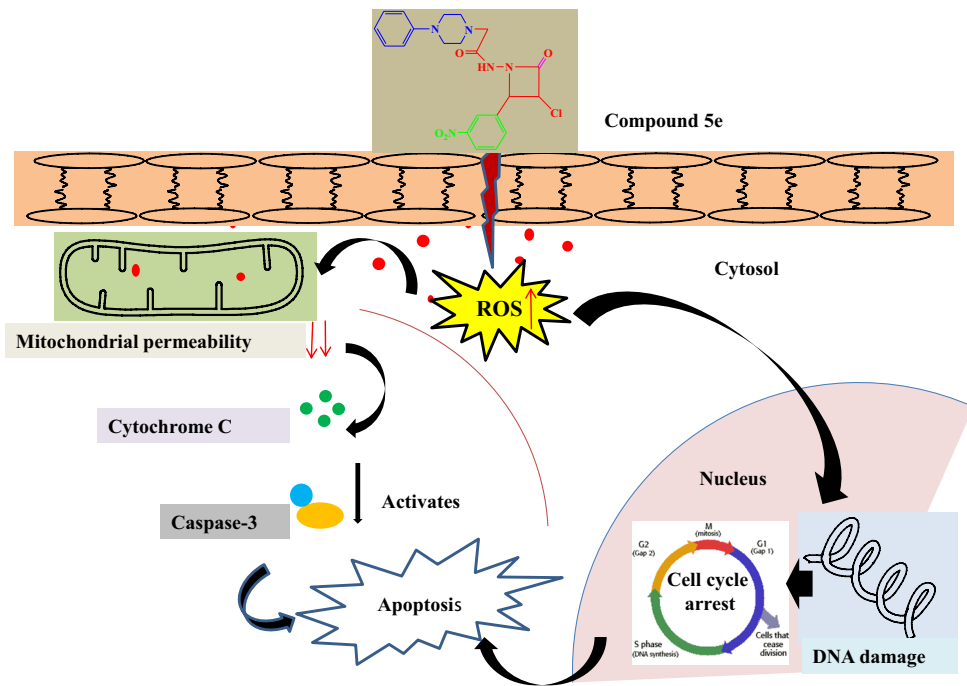


Fig. 8 a HeLa cells exposed to different concentrations of **5e** for 24 h then total protein and cytosolic protein extract were analyzed by Western blotting for cytochrome *c* in cytosolic protein fraction and caspase-3 in total cells protein extract. **b** Bar graph representing the

fold changes in the protein expression compared to loading control β-actin. Data expressed as mean ± SEM of triplicates. ****p* < 0.001 and *****p* < 0.0001 significant vs. control

Fig. 9 Proposed mechanism for induction of apoptosis by *N*-(3-chloro-2-(3-nitrophenyl)-4-oxoazetidin-1-yl)-2-(4-phenylpiperazin-1-yl) acetamide (**5e**) in human cervical cancer cell lines (HeLa)



cancer cells encourage us to further exploit its effect at cellular level, principally targeting the molecular mechanism involve in induction of apoptosis.

Recent studies have described the cytotoxic effect of some piperazine derivatives like β-elemene piperazine, 1,4-bis-(4-(1H-benzo[d]imidazol-2-yl-phenyl)) piperazine, chloroalkyl

piperazine and 6-(4 substituted piperazine-1-yl)-9-(β -D-ribofuranosyl) purine in several cancer cells via apoptosis induction, although, these derivatives activated only extrinsic pathway of apoptosis [28]. On the other hand, 2-azetidinones derivatives used in the preparation of some of anticancer drugs like paclitaxel (Taxol), docetaxel (Taxotere) and also exhibits anti-proliferation by inducing apoptosis in many human cancer cell lines such as breast, prostate and head and neck involving cell cycle arrest and caspase activation, however the mechanism remains unclear [29]. We herein demonstrate the possible mechanism of action of *N*-(3-chloro-2-(3-nitrophenyl)-4-oxoazetidin-1-yl)-2-(4-phenylpiperazin-1-yl) acetamide (**5e**) compound (conjugate of piperazine/2-azetidinone) (Fig. 1) in human cervical cancer cell (HeLa) via inducing apoptosis through oxidative stress. Our investigations provide the better understanding of the mechanism of action of compound **5e** and basis for the future development of drug for cervical cancer.

Apoptosis is prime target for many anticancer drugs according to the various reports [30, 31]. In the present study, the changes in cell morphology reveal that compound **5e** is cytotoxic and causes cell death in a concentration dependent manner (Fig. 2). Cells undergo apoptosis and inhibit the proliferation within 24 h of treatment. This was further shown through colony formation assay that displayed reduction in number and size of colonies (Fig. 3) [32]. We evaluated PS externalization, DNA fragmentation, ROS production, variation in mitochondrial membrane potential, translocation of cytochrome-*c* (cyt-*c*) and activation of caspases 3 as mediators of apoptosis. Therefore, we suggest the involvement of mitochondria mediated apoptotic pathway in compound **5e** induced HeLa cells (Fig. 9).

Evaluation of membrane blebbing and condensation of chromatin through AO/EtBr staining demonstrated the morphological changes significant to the apoptotic event (Fig. 5e) [31]. It is evident that on increasing the concentration of compound **5e** from 12.5 to 50 μ g/ml, the shift from early to the late stage of apoptotic events occurred, suggesting that treating HeLa cancer cells at higher concentrations of compound **5e** can induce necrosis in these cells (Fig. 5c, d) [33]. To further support the occurrence of apoptosis, we carried out cell cycle analysis in the HeLa cancer cells through PI staining [34]. On analyzing the various cell cycle phases, increase in the population of G2/M phase was observed with concomitant decrease in sub-G1 phase. These investigations confirm that cell death is initiated by apoptosis (Fig. 5a, b) [35]. Besides cell death compound **5e** was found to be effective in inhibiting the migration potential of the HeLa cells in vitro. Migration of cells is an important factor in cancer as it plays a major role in tumor progression and metastatic cascade. A substantial decrease of HeLa cell migration was noticed in vitro at $\frac{1}{2} \times IC_{50}$, IC_{50} and $2 \times IC_{50}$ concentrations of compound **5e** (Fig. 4a, b) [36].

Mitochondria are the chief source of ROS regulating the viability of cells. Our finding showed that ROS generation

increased extensively in HeLa cells (Fig. 6). Increase of ROS beyond a threshold damage DNA through activation of mitochondrial-related apoptotic signaling and also lead to mitochondrial dysfunction as shown by decrease in the mitochondria membrane potential in HeLa cells treated with compound **5e** (Fig. 7a, b) [37]. Disruption of mitochondrial membrane potential released cytochrome *c* which in turn, activates executioners of caspases, ultimately leading to cell death/DNA fragmentation (Fig. 5f) [38]. From western blot analysis it is reveal that compound **5e** enhance translocation of cytochrome *c* into cytosol leading to activation of caspase-3 (Fig. 8a, b). Thus, compound **5e** can be expected as a potent inducer of morphological variations involving apoptotic molecular events in the HeLa cancer cells related with its cytotoxic potential.

Conclusion

Our results revealed that compound **5e** (*N*-(3-chloro-2-(3-nitrophenyl)-4-oxoazetidin-1-yl)-2-(4-phenylpiperazin-1-yl) acetamide) inhibited the growth of HeLa cervical cancer cells by bringing apoptosis through ROS-mediated mitochondrial pathway. However, further investigation of its in vivo activity is required to explore its tumor reducing potential.

Acknowledgements The research work has been funded by UGC (F no-43-172/2014 (SR)).

Compliance with ethical standards

Conflict of interest All authors declare no conflict of interest.

Ethical approval This article has no studies concerned with human participants or animals.

References

1. Khazaei S, Ramachandran V, Abdul Hamid R, Esa NM, Etemad A, Moradipoor S, Ismail P (2017) Flower extract of *Allium atroviolaceum* triggered apoptosis, activated caspase-3 and down-regulated antiapoptotic Bcl-2 gene in HeLa cancer cell line. Biomed Pharmacother 89:1216–1226
2. World Health Organization (2014) GLOBOCAN2012: estimated cancer incidence, mortality and prevalence worldwide in 2012. International agency for research on cancer, population fact sheets (Islamic Republic of Iran)
3. Fulda S (2009) Tumor resistance to apoptosis. Int J Cancer 124:511–515
4. Thangam R, Sathuvan M, Poongodi A, Suresh V, Pazhanichamy K, Sivasubramanian S, Kanipandian N, Ganesan N, Rengasamy R, Thirumurugan R (2014) Activation of intrinsic apoptotic signaling pathway in cancer cells by *Cymbopogon citratus* polysaccharide fractions. Carbohydr Polym 107:138–150

5. Alshatwi AA, Periasamy VS, Athinarayanan J, Elango R (2016) Synergistic anticancer activity of dietary tea polyphenols and bleomycin hydrochloride in human cervical cancer cell: caspase-dependent and independent apoptotic pathways. *Chem Biol Interact* 247:1–10
6. Ahmed W, Van Etten RA (2013) Signal transduction in the chronic leukemias: implications for targeted therapies. *Curr Hematol Malig Rep* 8:71–80
7. Asif M (2015) Piperazine and pyrazine containing molecules and their diverse pharmacological activities. *Int J Adv Sci Res* 1:05–11
8. Berkheij M, van der Sluis L, Sewing C, den Boer DJ, Terpstra JW, Hiemstra H, Bakker WII, van den Hoogenband A, van Maarseveen JH (2005) Synthesis of 2-substituted piperazines via direct α -lithiation. *Tetrahedron Lett* 46:2369–2371
9. Wilson WD, Barton HJ, Tanius FA, Kong S-B, Streckowski L (1990) The interaction with DNA of unfused aromatic systems containing terminal piperazino substituents: intercalation and groove-binding. *Biophys Chem* 35:227–243
10. Gillet R, Jeannesson P, Sefraoui H, Arnould-Guerin M-L, Kirkiacharian S, Jardillier J-C, Pieri F (1997) Piperazine derivatives of butyric acid as differentiating agents in human leukemic cells. *Cancer Chemother Pharmacol* 41:252–255
11. Upadhyaya RS, Sinha N, Jain S, Kishore N, Chandra R, Arora SK (2004) Optically active antifungal azoles: synthesis and antifungal activity of (2R, 3S)-2-(2, 4-difluorophenyl)-3-(5-{2-[4-aryl-piperazin-1-yl]-ethyl}-tetrazol-2-yl/1-yl)-1-[1, 2, 4]-triazol-1-ylbutan-2-ol. *Bioorg Med Chem* 12:2225–2238
12. Chaudhary P, Kumar R, Verma AK, Singh D, Yadav V, Chhillar AK, Sharma G, Chandra R (2006) Synthesis and antimicrobial activity of *N*-alkyl and *N*-aryl piperazine derivatives. *Bioorg Med Chem* 14:1819–1826
13. Yoshida M, Maehara Y, Sugimachi K (1999) MST-16, a novel bis-dioxopiperazine anticancer agent, ameliorates doxorubicin-induced acute toxicity while maintaining antitumor efficacy. *Clin Cancer Res* 5:4295–4300
14. Hatnapure GD, Keche AP, Rodge AH, Birajdar SS, Tale RH, Kamble VM (2012) Synthesis and biological evaluation of novel piperazine derivatives of flavone as potent anti-inflammatory and antimicrobial agent. *Bioorg Med Chem Lett* 22:6385–6390
15. Shaquiquzzaman M, Verma G, Marella A, Akhter M, Akhtar W, Khan MF, Tasneem S, Alam MM (2015) Piperazine scaffold: a remarkable tool in generation of diverse pharmacological agents. *Eur J Med Chem* 102:487–529
16. Sun J (2017) Discovery of a series of 1,3,4-oxadiazole-2(3H)-thione derivatives containing piperazine skeleton as potential FAK inhibitors. *Bioorg Med Chem Lett* 25:2593–2600
17. Guo FJ, Sun J, Gao LL, Wang XY, Zhang Y, Qian SS, Zhu HL (2015) Discovery of phenylpiperazine derivatives as IGF-1R inhibitor with potent antiproliferative properties in vitro. *Bioorg Med Chem Lett* 25:1067–1071
18. da Silva DD, Silva MJ, Moreira P, Martins MJ, Valente MJ, Carvalho F, de Lourdes Bastos M, Carmo H (2016) In vitro hepatotoxicity of 'Legal X': the combination of 1 benzylpiperazine (BZP) and 1 (m trifluoromethylphenyl) piperazine (TFMPP) triggers oxidative stress, mitochondrial impairment and apoptosis. Springer, Heidelberg
19. Mehta PD, Sengar NP, Pathak AK (2010) 2-Azetidinone—a new profile of various pharmacological activities. *Eur J Med Chem* 45:5541–5560
20. Arya N, Jagdale AY, Patil TA, Yeramwar SS, Holikatti SS, Dwivedi J, Shishoo CJ, Jain KS (2014) The chemistry and biological potential of azetidin-2-ones. *Eur J Med Chem* 74:619–656
21. Smith DM, Kazi A, Smith L, Long TE, Heldreth B, Turos E, Dou QP (2002) A novel beta-lactam antibiotic activates tumor cell apoptotic program by inducing DNA damage. *Mol Pharmacol* 61:1348–1358
22. Dhivya R (2015) In vitro antiproliferative and apoptosis-inducing properties of a mononuclear copper (II) complex with dppz ligand, $i = n$ two genotypically different breast cancer cell lines. Springer, New York
23. Wani MY, Ahmad A, Shiekh RA, Al-Ghamdi KJ, Sobral AJ (2015) Imidazole clubbed 1,3,4-oxadiazole derivatives as potential antifungal agents. *Bioorg Med Chem* 23:4172–4180
24. Unver Y, Sancak K, Celik F, Birinci E, Kucuk M, Soyulu S, Burnaz NA (2014) New thiophene-1,2,4-triazole-5(3)-ones: highly bioactive thiosemicarbazides, structures of Schiff bases and triazolethiols. *Eur J Med Chem* 84:639–650
25. O'Boyle NM, Greene LM, Bergin O, Fichet JB, McCabe T, Lloyd DG, Zisterer DM, Meegan MJ (2011) Synthesis, evaluation and structural studies of antiproliferative tubulin-targeting azetidin-2-ones. *Bioorg Med Chem* 19:2306–2325
26. Morris GM (1998) Automated docking using a Lamarckian genetic algorithm and an empirical binding free energy function. *J Comput Chem* 19:1639–1662
27. Cohen G, Sun X, Snowden R, Dinsdale D, Skilleter D (1992) Key morphological features of apoptosis may occur in the absence of internucleosomal DNA fragmentation. *Biochem J* 286:331–334
28. Yu Z, Wang R, Xu L, Xie S, Dong J, Jing Y (2011) β -Elemene piperazine derivatives induce apoptosis in human leukemia cells through downregulation of c-FLIP and generation of ROS. *PLoS ONE* 6:e15843
29. Geesala R, Gangasani JK, Budde M, Balasubramanian S, Vaidya JR, Das A (2016) 2-Azetidinones: synthesis and biological evaluation as potential anti-breast cancer agents. *Eur J Med Chem* 124:544–558
30. Shyam H, Singh N, Kaushik S, Sharma R, Balapure AK (2017) Centchroman induces redox-dependent apoptosis and cell-cycle arrest in human endometrial cancer cells. *Apoptosis* 22:570–584
31. Aarts M, Sharpe R, Garcia-Murillas I, Gevensleben H, Hurd MS, Shumway SD, Toniatti C, Ashworth A, Turner NC (2012) Forced mitotic entry of S-phase cells as a therapeutic strategy induced by inhibition of WEE1. *Cancer Discov* 2:524–539
32. Kumar R, Tiku A (2018) Galangin induces cell death by modulating the expression of glyoxalase-1 and Nrf-2 in HeLa cells. *Chem Biol Interact* 279:1–9
33. Tentner AR, Lee MJ, Ostheimer GJ, Samson LD, Lauffenburger DA, Yaffe MB (2012) Combined experimental and computational analysis of DNA damage signaling reveals context-dependent roles for Erk in apoptosis and G1/S arrest after genotoxic stress. *Mol Syst Biol* 8, 568
34. Gasparri F, Cappella P, Galvani A (2006) Multiparametric cell cycle analysis by automated microscopy. *J Biomol Screen* 11:586–598
35. Liu Y-J, Liang Z-H, Hong X-L, Li Z-Z, Yao J-H, Huang H-L (2012) Synthesis, characterization, cytotoxicity, apoptotic inducing activity, cellular uptake, interaction of DNA binding and antioxidant activity studies of ruthenium (II) complexes. *Inorg Chim Acta* 387:117–124
36. Khanam R, Ahmad K, Hejazi II, Siddique IA, Kumar V, Bhat AR, Azam A, Athar F (2017) Inhibitory growth evaluation and apoptosis induction in MCF-7 cancer cells by new 5-aryl-2-butylthio-1,3,4-oxadiazole derivatives. *Cancer Chemother Pharmacol* 80:1027–1042
37. Hejazi II, Khanam R, Mehdi SH, Bhat AR, Rizvi MMA, Islam A, Thakur SC, Athar F (2017) New insights into the antioxidant and apoptotic potential of *Glycyrrhiza glabra* L. during hydrogen peroxide mediated oxidative stress: an in vitro and in silico evaluation. *Biomed Pharmacother* 94:265–279
38. Simon HU, Haj-Yehia A, Levi-Schaffer F (2000) Role of reactive oxygen species (ROS) in apoptosis induction. *Apoptosis* 5:415–418